MQW design parameter variation in a 1.5 μm wavelength InP-based LW-VCSEL

K. Kumarajah[2], Menon, P. S.[1], Ismail, M.[2], Yeop, B. Y.[1] & Shaari, S.[1]
[1]Institute of Microengineering and Nanoelectronics,
[2]Department of Electric, Electronics and System Engineering, Faculty of Engineering and Built Environment,
Universiti Kebangsaan Malaysia,
43600 UKM Bangi, Selangor
MALAYSIA.
susi@eng.ukm.my, http://www.ukm.my/imen

Abstract: - Long-wavelength vertical-cavity surface-emitting lasers (LW-VCSEL) have profound advantages compared to traditional edge-emitting lasers and its commercialization is gaining momentum as the local and access network in optical communication system expands. In this paper, we present the design parameter variations of multi quantum wells (MQW) in the active region of an InP-based long-wavelength vertical-cavity surface emitting laser (LW-VCSEL) utilizing an air-post design. The MQW and barrier thickness were varied and their effect on the device threshold current, optical power, gain, lattice temperature, peak wavelength and reflectivity were analysed and presented. Quantum well thickness of 5.5 nm and barrier thickness of 8 nm gives the optimum threshold current of 0.579 mA, optical power output of 4.2 mW, modal gain of 27 cm^{-1}, lattice temperature of 310.6 K and peak wavelength of 1.562 μm.

Key-Words: - VCSEL, MQW, InGaAsP, threshold current, gain, air-post

1 Introduction

Semiconductor diode lasers can be used in a variety of applications including telecommunications, displays, solid-state lighting, sensing and printing [1]-[3]. Vertical-cavity surface-emitting lasers (VCSELs) are attractive because of their compactness, low power consumption, circular output beam, dense packaging, and low production cost in comparison to conventional facet emitting lasers [4]. Furthermore, as deployment of fiber-to-the premises (FTTP) becomes more commonplace, the market for low-cost VCSELs also increases dramatically [5]. Long-wavelength VCSELs (LW-VCSEL) at 1.3 μm and 1.55 μm are of particular interest because they permit higher bit rates over longer distances while persevering the cost factor especially in access and backbone optical communication networks [6].

Currently, there are three main approaches being used in LW-VCSEL design. The first approach is an all-epitaxial wafer comprising of quarter-wavelength layers of InAlGaAs/InAlAs (InP) top and bottom distributed Bragg reflectors (DBRs) and active cavity region. In the second approach an InAlGaAs/InAlAs (InP) DBR is combined with a dielectric DBR. And finally, in the third approach, the InAlGaAs/InP active cavity is combined with wafer-fused AlGaAs/GaAs DBRs. For each one of these approaches, the maximum single-mode output power was 0.5 mW (70^0C), 1.4 mW (80^0C) and 2.5 mW respectively(80^0C) [7].

In the past, some VCSEL devices developed using the wafer fusion method have achieved continuous wave (CW) operation above 100^0C at 1.55 μm at a threshold current and voltage of 1 mA and 2.4V respectively [8]. Various other researchers have also employed the wafer-fusion method to take advantage of the high gain InP-based active region and high quality GaAs/AlGaAs DBRs [9]-[20]. Long-wavelength (LW) VCSELs normally employ either InGaAsP, InGaAlAs or AlInGaAs as the active region in the multi quantum well (MQW) layer [21]-[23].

The MQW LW-VCSEL has a larger optical mode confinement factor compared to single-quantum-well (SQW) VCSELs, resulting in lower threshold current density. Further reduction of laser threshold current density can be achieved by using a strained QW active layer. The biaxial strain caused by the slight lattice mismatch between the two material systems alters the valence band edge by removing degeneracy of the heavy hole and the light hole, resulting in reduced transparency carrier density and increased modal gain and thus reduced

threshold current density [24]. Furthermore, a semiconductor laser using the quantum well effect has additional features such as narrow frequency band gain curve, less temperature dependence and frequency of emission that can be designed by the dimension of the wells [25].

The main challenge in developing VCSELs is the simultaneous demonstration of high-temperature, high-speed and high-power fundamental mode lasing [26]. Finding the optimum design can be expensive and time-consuming hence in this paper we employ a commercial numerical-based simulation software to assist in the device design and optimization [27]. A two-dimensional modeling and characterization of a 1.55-µm wavelength VCSEL incorporating an InGaAsP-InP active cavity and wafer bonded top and bottom AlGaAs-GaAs/ AlAs-GaAs DBRs was developed partially based on the simulated and experimental device fabricated in the past [28]-[30].

2 Theoretical Analysis

The basis of the simulation is to solve two-dimensional Poisson's equation and the continuity equations for electrons and holes. Poisson's equation which is given by [27]

$$\nabla \bullet (\in \nabla \Psi) = \rho \quad (1)$$

relates variations in electrostatic potential ψ to local charge densities ρ and the local permittivity ε. The continuity equations are given by [27]

$$\frac{\partial n}{\partial t} = G_n - R_n + \frac{1}{q}\nabla \cdot \vec{J}_n \quad (2)$$

$$\frac{\partial p}{\partial t} = G_p - R_p + \frac{1}{q}\nabla \cdot \vec{J}_p \quad (3)$$

where n and p are the electron and hole concentrations, J_n and J_p are the electron and hole current densities, G_n and G_p are the generation rates for electrons and holes, R_n and R_p are the recombination rates and q is the magnitude of the charge on an electron.

The basic semiconductor equations (1)-(3) are solved self-consistently together with the Helmholtz, lattice heat flow and the photon rate equations. Two-dimensional Helmholtz equation is solved to determine the transverse optical field profile using the effective frequency method (EFM) and it is given by [27]:

$$\nabla^2 E(r,z,\varphi) + \frac{\omega_0^2}{c^2}\varepsilon(r,z,\varphi,\omega)E(r,z,\varphi) = 0 \quad (4)$$

where ω is the frequency, $\varepsilon(r, z, \varphi, \omega)$ is the complex dielectric permittivity, $E(r, z, \varphi)$ is the optical electric field, and c is the speed of light in vacuum. The heat flow equation has the form [27]:

$$C\frac{\partial T_L}{\partial t} = \nabla(\kappa \nabla T_L) + H \quad (5)$$

where C is the heat capacitance per unit volume, κ is the thermal conductivity, H is the generation and T_L is the local lattice temperature. The photon rate equation is solved in order to obtain the modal photon density, S_m and is given by [27]:

$$\frac{dS_m}{dt} = \left(\frac{c}{N_{eff}}G_m - \frac{1}{\tau_{ph_m}} - \frac{cL}{N_{eff}}\right)S_m + R_{sp_m} \quad (6)$$

where G_m is the modal gain, R_{spm} is the modal spontaneous emission rate, L represents the losses in the laser, N_{eff} is the group effective refractive index, τ_{phm} is the modal photon lifetime and c is the speed of light in vacuum. Equations (1)-(6) provides an approach that can account for the mutual dependence of electrical, optical and thermal phenomena in the development of a comprehensive VCSEL model.

The default energy bandgap for the InP lattice matched $In_{1-x}Ga_xAs_yP_{1-y}$ system used in this modeling is given by [27]:

$$\begin{aligned} E_g &= 1.35 + (0.642 + 0.758x)x + (0.101y \\ &- 1.101)y - (0.28x - 0.109y + 0.159)xy \end{aligned} \quad (7)$$

where x and y are the respective mole fraction for the III-V material.

The energy levels E_q of a particle of mass m confined to a one-dimensional infinite rectangular well of full width d are determined by solving the time-independent Schrodinger equation [31].

$$E_q = \frac{\hbar(q\pi / d)^2}{2m} \quad (8)$$

where q=1,2,……. This means the smaller the width of the quantum well, the larger the separation between adjacent energy levels.

The change in quantum well or barrier thickness affects the total effective length of the active or cavity region L_{eff}. This in turn affects the longitudinal mode spacing ($\Delta\lambda_m$) estimation given by [32]:

$$\Delta\lambda_m \approx \frac{\lambda^2}{2L_{eff}\langle \bar{n}_{gr} \rangle} \quad (9)$$

3 Device Design

The basic structure of a VCSEL is shown as in Fig. 1. It comprises of a cavity that is formed by two reflecting mirrors in the vertical direction composed of stacks of alternating low and high reflecting index materials. These highly reflecting structures are called distributed Bragg reflectors (DBRs) and require the thickness of each of the layers to be exactly a quarter of the desired lasing wavelength in the material. Similar to the formation of very thin and smooth heterostructures, like quantum wells for the gain medium, these layers in the DBRs need to be of very high quality [33].

Fig 1 shows the schematic design of the air-post wafer-bonded GaAs-based 1.5 µm VCSEL device. In this structure, the multi-quantum well (MQW) active region consists of six 5.5-nm thick $In_{0.76}Ga_{0.24}As_{0.82}P_{0.18}$ quantum wells and 8-nm thick $In_{0.48}Ga_{0.52}As_{0.82}P_{0.18}$ barriers. The MQWs are embedded in InP spacer layers that have been extended by thin GaAs layers on top of each fused mirror to increase emission wavelength. Alternating high- and low-refractive index layers of $GaAs/Al_{0.33}Ga_{0.67}As$ form the top 30-period p-type DBR whereas the bottom n-type DBR mirror is formed with 28-periods of GaAs/AlAs layers.

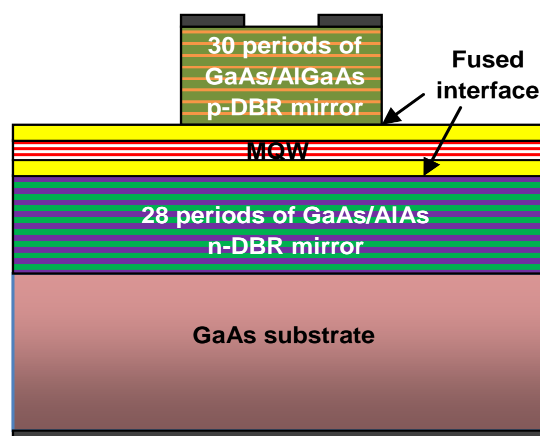

Fig.1 Schematic structure of the VCSEL device.

4 Simulation Results

The energy bandgap for the quantum well and barrier material is 0.74 eV and 1.14 eV respectively; calculated using Eq. 7. The MQW parameters evaluated in this paper are the well thickness and the barrier thickness. The cavity thickness which includes the active region and the spacer layers is 705 nm. The total active layer thickness is 89 nm. The device is assumed to be exposed to an environmental temperature of 300 K. The quantum well thickness was increased from 3.5 nm to 9.5 nm while maintaining the quantum well barrier thickness at 8 nm and quantity of quantum well of 6. The quantum well barrier thickness was increased from 4 nm to 12 nm while maintaining the quantum well thickness at 5.5 nm and quantum well quantity at 6. The thickness of the top and bottom DBR layers as well as the total cavity thickness was maintained to be the same by reducing/increasing the thickness of the n-InP spacer layers.

Table 1 summarizes the total active layer and cavity thickness with the variation in the quantum well and barrier thicknesses. Quantum wells can be classified as weakly coupled quantum wells or strongly coupled quantum wells depending on the thickness of the both the quantum wells and the barrier. Thin and narrow barriers produce strongly coupled quantum wells and enhance electron tunneling between wells. On the other hand, a weakly coupled quantum well will have fixed amounts of electrons residing in it with quantized energy values.

Quantum Well thickness (nm)	Quantity of quantum well	Barrier thickness (nm)	Quantity of barriers	Total active layer thickness (nm)	n-InP Spacer layer	Total cavity layer thickness (nm)
3.5	6	8	7	77	0.27	705
4.5	6	8	7	83	0.264	705
5.5	6	8	7	89	0.258	705
6.5	6	8	7	95	0.252	705
7.5	6	8	7	101	0.246	705
8.5	6	8	7	107	0.24	705
9.5	6	8	7	113	0.234	705
5.5	6	4	7	61	0.286	705
5.5	6	5	7	68	0.279	705
5.5	6	6	7	75	0.272	705
5.5	6	7	7	82	0.265	705
5.5	6	8	7	89	0.258	705
5.5	6	9	7	96	0.251	705
5.5	6	10	7	103	0.244	705
5.5	6	11	7	110	0.237	705
5.5	6	12	7	117	0.23	705

Table 1 Total active layer and cavity layer thickness for different quantum well and barrier thickness

Fig. 2-Fig. 7 show the effect of quantum well thickness on the VCSEL's voltage-current (V-I), optical power-current (L-I), gain-current, lattice temperature-current (T-I), wavelength-current and reflectivity-current curves. The quantum well thickness was increased from 3.5 nm to 9.5 nm while maintaining the quantum well barrier thickness at 8 nm and quantity of quantum well of 6.

In Fig. 2, when the voltage in increased beyond the threshold voltage, there is only minor increment in the electrical current. The I-V characteristics follow the form of $V \approx V_k + R_S I$ where V_k is related to the quasi-Fermi energies (equivalent to ~0.9 V) and R_S denotes the differential series resistance where R_S values are between 202.5-203.4 Ω at V=3V for all quantum well thicknesses. The corresponding electrical current decreases from 14.8 mA (d_{QW}=3.5 nm, V=3V) to 14.7 mA (d_{QW}=9.5 nm, V=3V) as the quantum well thickness is increased due to the increment in active region volume which consequently reduces the carrier generation rate. However, the reduction in the electrical current is small (<1%) since the quantum well barrier is thick enough to avoid carrier tunneling to occur between the wells and each well can still be treated as a separate carrier reservoir.

The L-I curve in Fig. 3 shows increment in the optical power output at higher current values as the quantum well thickness is increased. The light output power is governed by $P=\eta(\hbar v/q)(I-I_{th})$ where η is the differential quantum efficiency, hv and q are the photon energy and electron charge, I is the driving current and I_{th} is the threshold current. Quantum efficiencies ranging from 17.7% (d_{QW}=3.5 nm at 1.5 V) up to 18.5% (d_{QW}=9.5 nm at 1.5 V) was achieved where the peak power achieved at V=3V ranges from 4.9 mW (d_{QW}=3.5 nm) to 5.2 mW (d_{QW}=9.5 nm). As the quantum well thickness is increased, the separation between adjacent quantum energy levels in the well reduces as given by Eq. 8 and this in turn increases the recombination rate to produce higher photon densities which contribute to the higher optical power observed at higher operating voltages and thicker quantum wells.

The gain curves shown in Fig. 4 show a decreasing value from 26.7 cm^{-1} (d_{QW}=3.5 nm, V=1.5 V) to 23.2 cm^{-1} (d_{QW}=9.5 nm, V=1.5 V). Since the gain for a certain photon energy is proportional to the joint density of states of the quantum wells, increment in the quantum well thickness reduces the density of states and subsequently the material gain.

Self heating in VCSEL devices during CW operation primarily affects the distribution function of the carriers and the bandgap of the semiconductor, and hence a host of other parameters such as carrier densities and refractive index. These parameters in turn alter the gain distribution, increase various dark carrier recombination processes and induce a temperature related resonant wavelength shift, all of which are detrimental to laser output performance [34]. Hence, the VCSEL device was exposed to an external temperature of 300K and Fig. 5 is an analysis of this phenomenon and the graph shows that the lattice temperature increases linearly with the injection current. Above threshold, the lattice temperature increases between 10K and 11K at the maximum voltage of 3 V (corresponding to injection currents of 14.7-14.8 mA).

Fig. 6 exhibits the increase in the peak wavelength upon increment of the quantum well thickness. Although the total cavity thickness was maintained to be the same at 705 nm, the increasing thickness of the active region causes the peak resonance wavelength to nudge according to $nL=m\lambda/2$ where n is the effective refractive index of the active region, L is the total effective region thickness, m is the propagating mode (in this case, $m=1$ for single-mode operation) and λ is the peak resonance wavelength. When the quantum well thickness is increased, the peak resonance wavelength increases from 1.562µm (d_{QW}=3.5 nm at 1.5 V) to 1.565µm (d_{QW}=9.5 nm at 1.5 V).

The effects of quantum well thickness on the VCSEL reflectivity is displayed in Fig. 7. While the top DBR mirror reflectivity is maintained at

99.84%, the bottom DBR mirror reflectivity increases from 99.78% (d_{QW}=3.5 nm at 1.5 V) to 99.83% (d_{QW}=3.5 nm at 1.5 V). Again, this is due to the shift in the peak resonance with respect to the standing wave pattern. The lower rear mirror reflectivity compared to the higher top mirror reflectivity indicates that the VCSEL is a bottom-emitting laser.

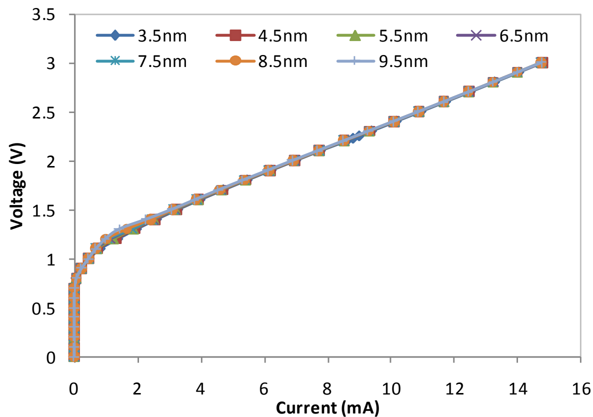

Fig. 2 Effect of quantum well thickness on the voltage-current (V-I) curve

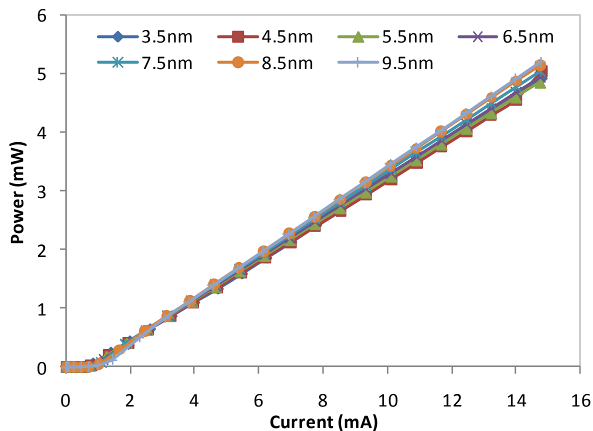

Fig. 3 Effect of quantum well thickness on the optical power-current (L-I) curve

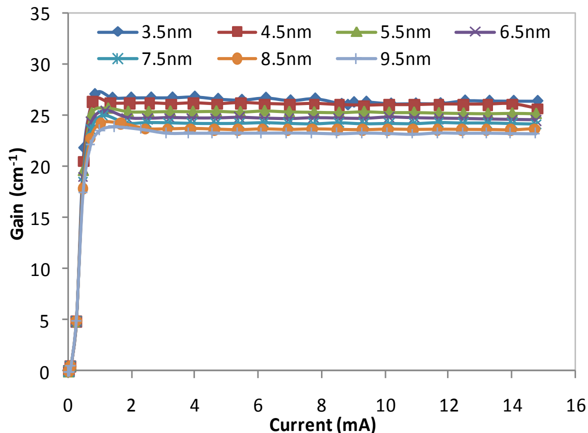

Fig. 4 Effect of quantum well thickness on the gain-current (Gain-I) curve

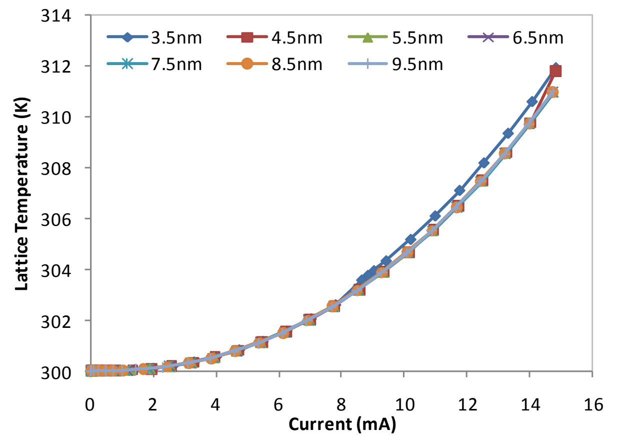

Fig. 5 Effect of quantum well thickness on the temperature-current (Temp-I) curve

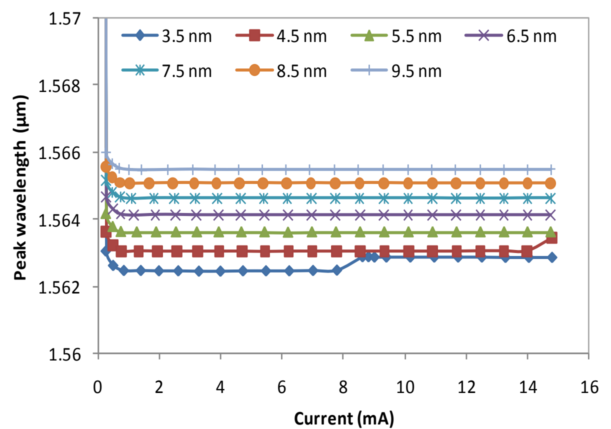

Fig. 6 Effect of quantum well thickness on the peak wavelength-current (λ-I) curve

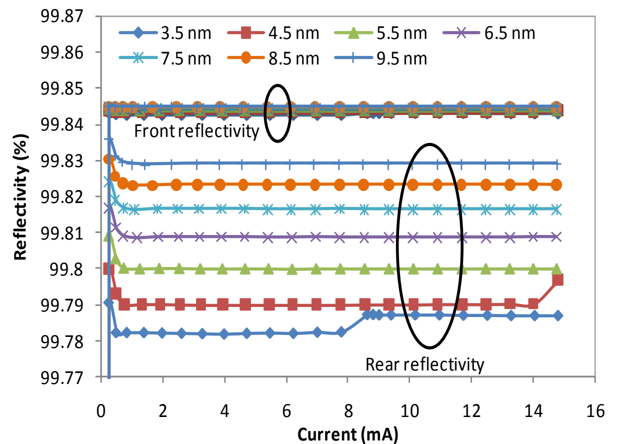

Fig. 7 Effect of quantum well thickness on the reflectivity-current (R-I) curve

Fig. 8-Fig. 13 show the effect of quantum well barrier thickness on the VCSEL's voltage-current (V-I), optical power-current (L-I), gain-current, lattice temperature-current (T-I), wavelength-

current and reflectivity-current curves. The quantum well barrier thickness was increased from 4 nm to 12 nm while maintaining the quantum well thickness at 5.5 nm and quantum well quantity at 6.

In Fig. 8, d_{QWB} values > 5 nm show linear increment of the electrical current with bias voltage above threshold where I=14.7 mA when V=3V. For smaller barrier thicknesses (d_{QWB}=4 nm), the electrical current is higher (16 mA) probably due to some electron tunneling between wells through the thin barrier walls. The differential series resistance is about 203.4 Ω at V=3V.

The L-I curve in Fig. 9 shows increment in the optical power output as the quantum well barrier thickness is increased. No lasing is obtained for d_{QWB}=4 nm probably because of electron tunneling between wells which reduces the carrier recombination rate and subsequently the photon generation rate. Quantum efficiencies ranging from 14.5% (d_{QWB}=5 nm at 1.5 V) up to 20.5% (d_{QWB}=12 nm at 1.5 V) was achieved where the peak power achieved at V=3V ranges from 4.4 mW (d_{QWB}=5 nm) to 5.4 mW (d_{QWB}=12 nm); an increment of 22.7%. A thicker quantum well barrier minimizes electron tunneling between wells hence more electrons are available for the recombination process to produce a larger photon density.

The gain curves shown in Fig. 10 show a decreasing value from 27.6 cm^{-1} (d_{QWB}=5 nm, V=1.5 V) to 23.1 cm^{-1} (d_{QWB}=12 nm, V=1.5 V). The decrement in the gain is due to the offset between the standing wave pattern and peak gain in the active region when the active region thickens as the barrier thickness is increased.

Fig. 11 shows the effect of quantum well barrier thickness on the temperature-current curve. With the exception of d_{QWB}=4 nm, all the other barrier thicknesses show lattice temperature increment between 10K and 11K at the maximum voltage of 3 V (corresponding to injection currents of 14.7-14.8 mA) above threshold.

The trend seen in Fig. 6 is reproduced again in Fig. 12 which exhibits the increase in the peak wavelength upon increment of the quantum well barrier thickness. When the quantum well barrier thickness is increased, the peak resonance wavelength increases from 1.56μm (d_{QWB}=4 nm at 1.5 V) to 1.566μm (d_{QWB}=12 nm at 1.5 V).

The effects of quantum well barrier thickness on the VCSEL reflectivity is displayed Fig. 13. Again, while the front mirror reflectivity is maintained at 99.84%, the rear mirror reflectivity increases from 99.74% (d_{QWB}=4 nm at 1.5 V) to 99.83% (d_{QWB}=12 nm at 1.5 V). Again, this is due to the shift in the peak resonance with respect to the standing wave pattern due to the increasing thickness of the active region.

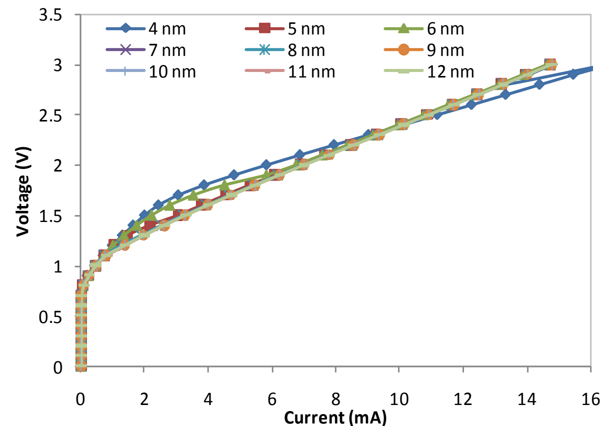

Fig. 8 Effect of quantum well barrier thickness on the voltage-current (V-I) curve

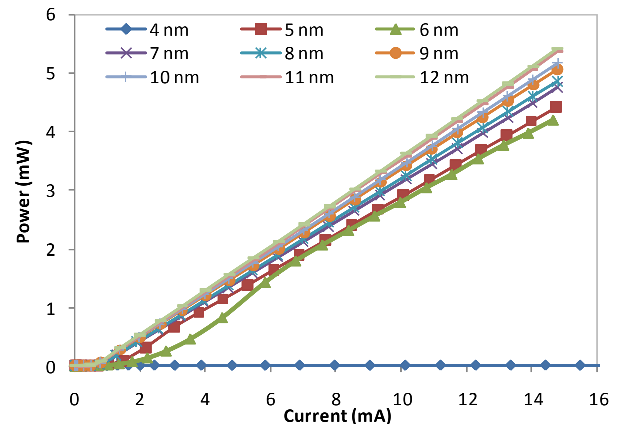

Fig. 9 Effect of quantum well barrier thickness on the optical power-current (L-I) curve

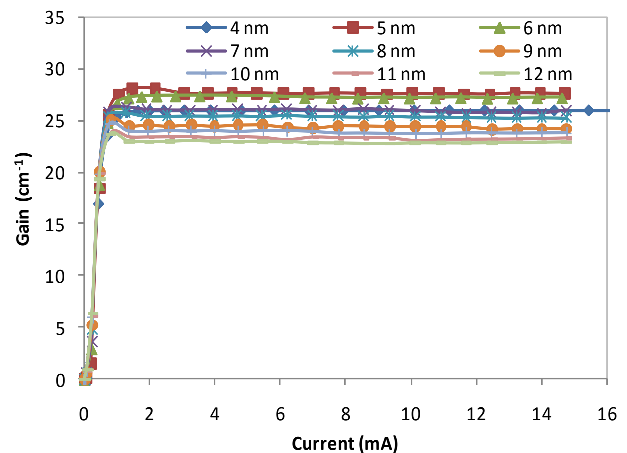

Fig. 10 Effect of quantum well barrier thickness on the gain-current (Gain-I) curve

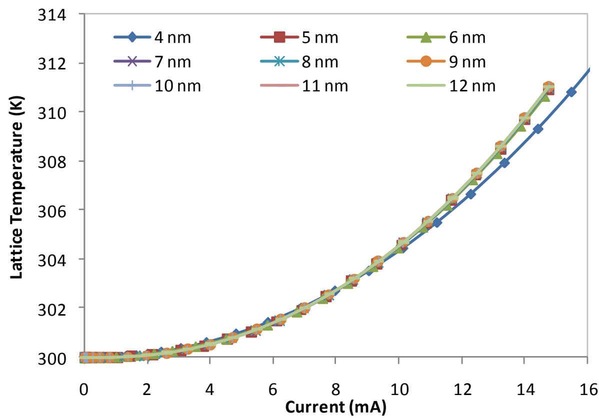

Fig. 11 Effect of quantum well barrier thickness on the temperature-current (Temp-I) curve

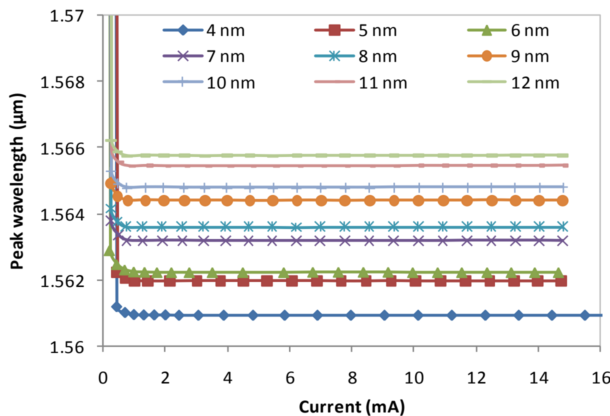

Fig. 12 Effect of quantum well barrier thickness on the peak wavelength-current (λ-I) curve

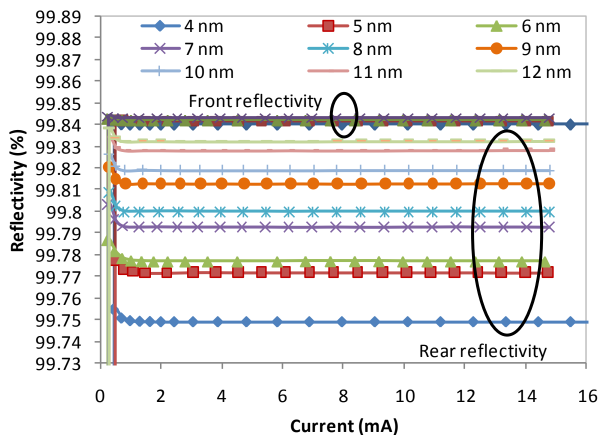

Fig. 13 Effect of quantum well thickness on the reflectivity-current (R-I) curve

Fig. 14 shows the effect of the barrier and QW thickness on the VCSEL threshold current, I_{th}. The lowest threshold current of 0.579 mA is achieved for d_{QW} = 5.5 nm (d_{QWB} =8 nm) whereas I_{th} is further reduced to 0.524 mA when d_{QW} =5.5 nm and d_{QWB} =12 nm. However, for thicker barrier regions the modal gain reduces (~ 23 cm^{-1}) as can be seen in Fig. 15 due to the shift in the cavity resonance spectral overlap of the laser gain region. An optimal QW should have thin QWs separated by thick barriers where coupling between wells is negligible. However, when both the QWs and barriers are thin, coupling between wells occur and a superlattice is formed instead and no lasing occurs in the device [24]. This explains the non-existant/non-ideal characteristic of the threshold current for thin QW and barriers (< 3.5 nm). For thicker QWs and barriers, the threshold current decreases due to increment in injected carriers in the QW and no coupling is formed between adjacent QWs enabling smoother carrier propagation.

The thickness of the QW and the barrier also has an effect on the lattice temperature as portrayed in Fig. 16. Assuming an external environmental temperature of 300K; for thicker barriers, lattice temperature increases due to the decrement of carrier injection efficiency with an increase in the propagation distance of the carriers. However, for thicker QWs, the lattice temperature shows gradual decrement due to the higher number of carriers involved in the spontaneous emission process [24].

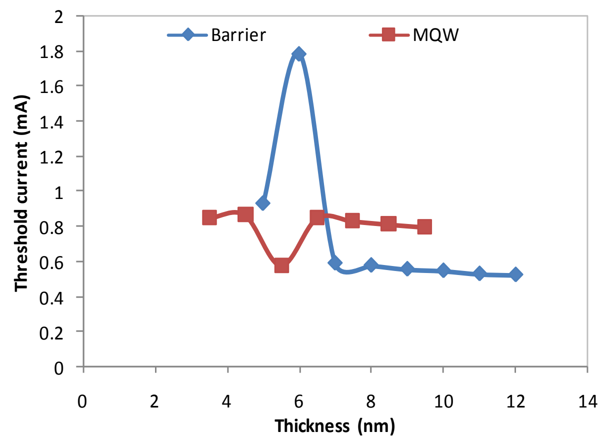

Fig. 14 Effect of QW and barrier thickness on threshold current.

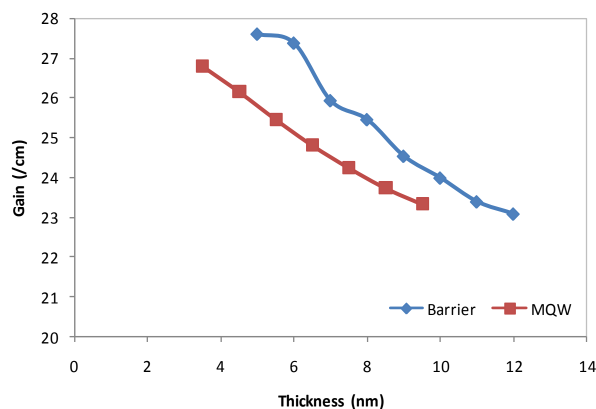

Fig. 15 Effect of QW and barrier thickness on gain (V=1.5V).

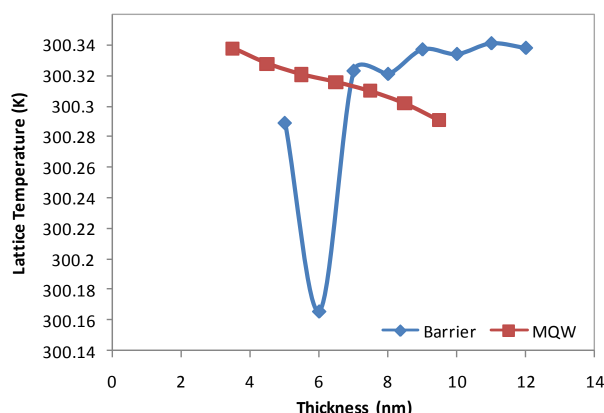

Fig. 16 Effect of QW and barrier thickness on lattice temperature (V=1.5V).

5 Conclusion

In this paper, we have shown that the quantum well and barrier thickness have a profound impact on the VCSEL threshold current, optical power output, modal gain, lattice temperature, peak wavelength and the reflectivity. Quantum well thickness of 5.5 nm and barrier thickness of 8 nm gives the optimum threshold current of 0.579 mA, optical power output of 4.2 mW, modal gain of 27 cm^{-1}, lattice temperature of 310.6 K and peak wavelength of 1.562 µm.

References:

[1] M. Mazalkova, "The laser satellites communications and laser noises", WSEAS Transactions on Communications, Vol.7, No. 8, 2008, pp. 872-881.

[2] E. A. Anagnostakis, "Wavefunction-engineering of the optoelectronic yield for intersubband THz-Laser nanodevices", WSEAS Transactions on Electronics, Vol. 5, No. 9, 2008, pp. 387-396.

[3] M. S. Mazalkova, "The system transfering between laser-satellites", WSEAS Transactions on Communications, Vol. 7, No. 3, 2008, pp. 152-159.

[4] A. Valle, M. Gýmez-Molina, and L. Pesquera, "Polarization Bistability in 1550 nm Wavelength Single-Mode Vertical-Cavity Surface-Emitting Lasers Subject to Orthogonal Optical Injection," IEEE Journal of Selected Topics in Quantum Electronics, vol. 14, 2008, pp. 895-902.

[5] W. Hofmann, E. Wong, G. Bhm, M. Ortsiefer, N. H. Zhu, and M. C. Amann, "1.55-µm VCSEL Arrays for High-Bandwidth WDM-PONs," IEEE Photonics Technology Letters, vol. 20, 2008, pp. 291-293

[6] P. Abraham, A. Karim, D. Lofgreen, Y.-J. Chiu, J. Piprek, and J. Bowers, "Wafer bonded 1.55 µm vertical-cavity lasers with continuous-wave operation up to 105 °C.," Applied Physics Letters, vol. 78, 2001, pp. 2632-2634.

[7] E. Kapon & A. Sirbu, Power-efficient answer, Nature Photonics, Vol. 3, 2009, pp. 27-29.

[8] A. Karim, J. Piprek, P. Abraham, D. Lofgreen, Y.-J. Chiu, and J. E. Bowers, "1.55-µm vertical-cavity laser arrays for wavelength-division multiplexing," IEEE Journal of Selected Topics in Quantum Electronics, vol. 7, 2001, pp. 178–183.

[9] J. J. Dudley, D. L. Crawford, J. E. Bowers, P. Silvestre, and G. Y. Robinson, "Temperature dependence and material properties of InGaAsP/InP mirrors," Fourth International Conference on in Indium Phosphide and Related Materials, 1992, pp. 666 – 669

[10] H. Wada, D. I. Babic, D. L. Crawford, J. J. Dudley, J. E. Bowers, E. L. Hu, J. L. Merz, B. I. Miller, U. Koren, and M. G. Young, "High-temperature pulsed operation of InGaAsP/InP surface emitting lasers," IEEE Transactions on Electron Devices, vol. 38, 1991, p. 2701.

[11] D. I. Babic and J. S. Piprek, K.; Mirin, R.P.; Margalit, N.M.; Mars, D.E.; Bowers, J.E.; Hu, E.L.;, "Design and analysis of double-fused 1.55-µm vertical-cavity lasers," IEEE Journal of Quantum Electronics, vol. 33, 1997, pp. 1369-1383.

[12] N. M. Margalit, J. Piprek, S. Zhang, D. I. Babic, K. Streubel, R. P. Mirin, J. R. Wesselmann, and J. E. Bowers, "64°C continuous-wave operation of 1.5-µm vertical-cavity laser," IEEE Journal of Selected Topics in Quantum Electronics, vol. 3, 1997, pp. 359-365.

[13] A. Keating, A. Black, A. Karim, Y.-J. Chiu, P. Abraham, C. Harder, E. Hu, and J. E. Bowers, "High-temperature optically pumped 1.55-µm VCSEL operating at 6 Gb/s," IEEE Photonics Technology Letters, vol. 12, 2000, pp. 116 – 118.

[14] S. Z. Zhang, N. M. Margalit, T. E. Reynolds, and J. E. Bowers, "1.54-µm vertical-cavity surface-emitting laser transmission at 2.5 Gb/s," IEEE Photonics Technology Letters, , vol. 9, 1997, pp. 374 - 376.

[15] M. Mehta, V. Robbins, S. Lester, D. Mars, D. Bour, F. Mertz, J. Miller, and J. E. Bowers, "High power, high speed, single-mode wafer-bonded AlInGaAs-based LW-VCSELs at 70/spl deg/C," in Optical Fiber Communication Conference, 2006 and the 2006 National Fiber Optic Engineers Conference. OFC, 2006, p. 3.

[16] M. Mehta, E. S. Bjorlin, and J. E. Bowers, "Calculated voltage characteristics for tunnel junctions in double cavity long-wavelength surface emitting lasers," Proceedings of the 4th International Conference in Numerical Simulation of Optoelectronic Devices. NUSOD '04., 2004, pp. 51 - 52.

[17] J. Geske, K.-G. Gan, Y. L. Okuno, J. Piprek, and J. E. Bowers, "Vertical-Cavity Surface-Emitting Laser Active Regions for Enhanced Performance With Optical Pumping," IEEE Journal of Quantum Electronics, vol. 40, 2004, pp. 1155-1162.

[18] J. Piprek, V. Jayaraman, M. Mehta, and J. E. Bowers, "Balanced optimization of 1.31 /spl mu/m tunnel-junction VCSELs," Proceedings of the IEEE/LEOS 3rd International Conference in Numerical Simulation of Semiconductor Optoelectronic Devices, NUSOD 2003., 2003, pp. 45 – 46.

[19] M. Mehta, V. Jayaraman, A. Jackson, S. Wu, Y. Okuno, J. Piprek, and J. E. Bowers, "134/spl deg/ C continuous-wave operation of a 1.33-/spl mu/m wafer-bonded VCSEL," Conference in Lasers and Electro-Optics, CLEO '03., 2003, p. 2.

[20] A. Keating, A. Black, A. Karim, Y.-J. Chiu, P. Abraham, C. Harder, E. Hu, and J. E. Bowers, "High-temperature optically pumped 1.55-µm VCSEL operating at 6 Gb/s," IEEE Photonics Technology Letters, vol. 12, 2000, pp. 116 - 118

[21] A. Karim, P. Abraham, D. Lofgreen, Y.-J. Chiu, J. Piprek, and J. Bowers, "Wafer bonded 1.55 µm vertical-cavity lasers with continuous-wave operation up to 105 °C.," Applied Physics Letters, vol. 78, 2001, pp. 2632-2634.

[22] W. Hofmann and M.-C. Amann, "Long-wavelength vertical-cavity surface-emitting lasers for high-speed applications and gas sensing," IET Optoelectronics, vol. 2, 2008, pp. 134-142.

[23] M. Mehta, D. Feezell, D. A. Buell, A. W. Jackson, L. A. Coldren, and J. E. Bowers, "Electrical design optimization of single-mode tunnel-junction-based long-wavelength VCSELs," IEEE Journal of Selected Topics in Quantum Electronics, vol. 42, 2006, pp. 675-682.

[24] E. Maass, Handbook of Fiber Optic Data Communication. CA: Academic Press, 1998.

[25] K. Iizuka, Elements of Photonics, Vol. II, New York: Wiley-Interscience, 2002

[26] J. Piprek, M. Mehta, and V. Jayaraman, "Design and Optimization of high-performance 1.3 um VCSELs," in Proceedings of SPIE, 2004.

[27] SILVACO International, ATLAS User's Manual, Version 5.12.0.R. USA, SILVACO International Incorporated, 2007.

[28] D. I. Babic, J. S. Piprek, K.; Mirin, R.P.; Margalit, N.M.; Mars, D.E.; Bowers, J.E.; Hu, E.L.;, "Design and analysis of double-fused 1.55-µm vertical-cavity lasers," IEEE Journal of Selected Topics in Quantum Electronics, vol. 33, 1997, pp. 1369-1383.

[29] K. Kandiah, P. S. Menon, & S. Shaari. "Design and modeling of a vertical-cavity surface-emitting laser (VCSEL)", Proceedings of the 2008 IEEE International Conference on Semiconductor Electronics, ICSE2008, 2008, pp. 297-301.

[30] K. Kandiah, M. Ismail, P. S. Menon, S. Shaari & B. Y. Majlis. Multi-quantum well design parameter variation in InP-based VCSEL. Proceedings of 8th WSEAS International Conference on Microelectronics, Nanoelectronics and Optoelectronics (MINO'09), 2009, pp. 115-117.

[31] B. E. A. Saleh & M. C. Teich, Fundamentals of Photonics, New York: Wiley, 1991

[32] H. Li & K. Iga, Vertical-Cavity Surface-Emitting Laser Devices, New York: Springer, 2002.

[33] C. Wilmsen, H. Temkin & L.A. Coldren, Vertical-Cavity Surface-Emitting Lasers, United Kingdom: Cambridge University Press, 1999.

[34] W.-C. Ng, Y. Liu, and K. Hess, "Lattice Temperature Model and Temperature Effects in Oxide-Confined VCSELs," Journal of

Computational Electronics, vol. 3, pp. 103-116, 2004.